Table 1　第1回入院時検査所見

Peripheral blood		Blood chemistry		Serology	
WBC	3,800 /μl	TP	4.9 g/dl (6.3—8.1)	RA	(−)
	(4,000—9,000)	Alb	1.9 g/dl (3.7—4.9)	ANA	(−)
Stab	3.0 %	LDH	492 IU/l (125—237)	Anti-DNA Ab	(−)
Seg	58.0 %	GOT	29 IU/l (9—38)	ANCA	(−)
Eo	0.0 %	GPT	13 IU/l (4—36)	HBs Ag	(−)
Bas	2.0 %	γ GTP	42 IU/l (4—68)	HCV Ab	(−)
Mo	14.0 %	ALP	179 IU/l (60—201)	HTLV-1 Ab	(−)
Ly	19.0 %	T-Bil	0.6 mg/dl (0.3—1.3)	CRP	7.0 mg/dl (< 0.3)
Atypical ly	4.0 %	BUN	15.8 mg/dl (9—31)	Ferritin	1,181 ng/ml (4—108)
RBC	248 × 10^4 /μl	Cr	0.55 mg/dl (0.4—0.9)	EPO	709 mIU/ml (16.6—37.5)
	(380—480 × 10^4)	Na	132 mEq/l (132—148)	sIL-2R	3,227 U/ml (167—497)
Hb	7.5 g/dl (12—16)	K	4.3 mEq/l (3.5—4.9)	EBV VCA-IgG	× 320 (0—10)
Ht	22.6 % (34—42)	Cl	100 mEq/l (96—108)	EBV VCA-IgM	< × 10 (0—10)
Reti	0.2 % (0.8—2.0)	Fe	101 μg/dl (40—162)	EA-IgG	< × 10 (0—10)
Plt	9.5 × 10^4 /μl	UIBC	120 μg/dl (126—358)	EBNA	× 20 (0—10)
	(14—40 × 10^4)	Glu	126 mg/dl (75—105)	parvo B19 IgM	0.13
				Flowcytometry	
				CD3/CD19	87/2
				CD4/CD8	0.37
				CD8 + DR +	60 %

Bone Marrow　normocellular bone marrow
NCC 5.7 × 10^4/μl, M/E 103.38, MgK 60
Erythroid series : Pro 0.0%, Baso 0.8%, Poly 0.0%, Ortho 0.0%, giant polyerythroblast (−)

Table 2　第2回入院時検査所見

Peripheral blood		Blood chemistry		Serology	
WBC	3,700 /μl	TP	5.6 g/dl (6.3—8.1)	CRP	6.5 mg/dl (< 0.3)
	(4,000—9,000)	Alb	2.6 g/dl (3.7—4.9)	Ferritin	2,523 ng/ml (4—108)
Stab	0.0 %	LDH	333 IU/l (125—237)	sIL-2R	1,877 U/ml (167—497)
Seg	62.0 %	GOT	27 IU/l (9—38)	EBV VCA-IgG	× 640 (0—10)
Eo	0.0 %	GPT	17 IU/l (4—36)	EBV VCA-IgM	< × 10 (0—10)
Bas	1.0 %	γ GTP	35 IU/l (4—68)	EA-IgG	< × 10 (0—10)
Mo	13.0 %	ALP	149 IU/l (60—201)	EBNA	× 40 (0—10)
Ly	20.0 %	T-Bil	0.6 mg/dl (0.3—1.3)		
Atypical ly	4.0 %	BUN	21.6 mg/dl (9—31)	Flowcytometry	
RBC	289 × 10^4 /μl	Cr	0.75 mg/dl (0.4—0.9)	CD3/CD19	80/3
	(380—480 × 10^4)	Na	135 mEq/l (132—148)	CD4/CD8	0.5
Hb	9.1 g/dl (12—16)	K	4.1 mEq/l (3.5—4.9)		
Ht	27.0 % (34—42)	Cl	103 mEq/l (96—108)		
Reti	1.7 % (0.8—2.0)	Fe	21 μg/dl (40—162)		
Plt	8.5 × 10^4 /μl	UIBC	143 μg/dl (126—358)		
	(14—40 × 10^4)	Glu	122 mg/dl (75—105)		

Bone Marrow　normocellular bone marrow
NCC 6.5 × 10^4/μl, M/E 1.52
Erythroid series : Pro 1.7%, Baso 6.1%, Poly 19.1%, Ortho 9.6%, giant polyerythroblast (−)
大型でN/C比中等度の細胞を多数認め（30～40%），これらの細胞はMPO陰性で核小体を有し，
細胞質のbasophiliaは強度で，細胞質内には空胞が多数存在する．
Immunological staining
CD20 (+), CD19 (+), CD3 (−), CD5 (−), CD10 (−), CD79a (+), λ dominant
EBER (−), LMP1 (−), EBNA2 (−), IgH/C-MYC : (−) (t(8 ; 14), t(8 ; 2), t(8 ; 22))

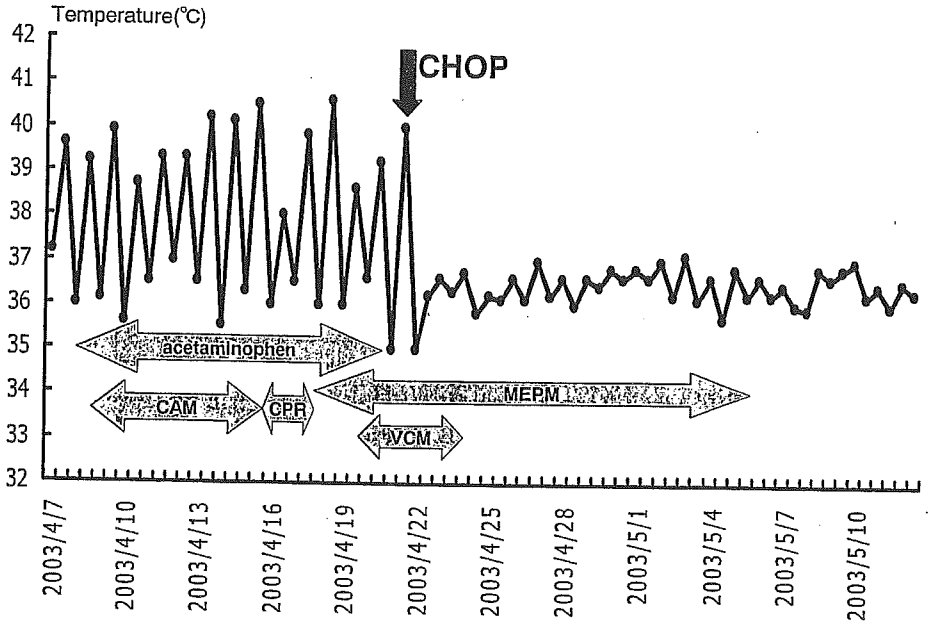

Fig. 1　第2回入院時の臨床経過．CAM：clarithromycin，CPR：cefpirome sulfate，VCM：vancomycin hydrochloride

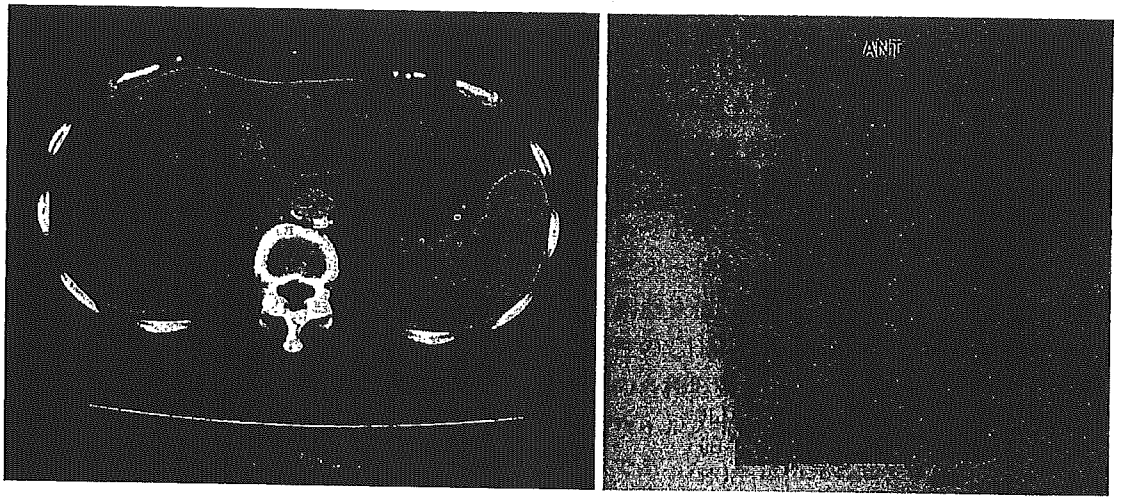

Fig. 2　第2回入院中に施行した腹部造影CT（図左）とガリウムシンチグラフィー（図右）．CTで脾臓内に低吸収域が散在し，ガリウムシンチグラフィーで相対的な脾臓の取り込み増加が認められる．

診断した．抗生剤を一時中止して熱型を観察したが，38℃以上の発熱が続き，再び抗生剤治療を行ったものの解熱は得られなかった．7月上旬に右季肋部痛，胆嚢腫脹，胆道系酵素上昇が認められ，胆嚢穿刺を行ったところ，それを契機に解熱し，CRPも低下した．解熱後，食事摂取良好となり8月下旬に独歩にて退院した．胆嚢炎のみで経過が説明できないため，リンパ増殖性疾患の可能性も考慮し脾摘も検討したが，診断確定には至らなかった．貧血に対しては適宜輸血を行い経過観察した．胆嚢穿刺から約1カ月経過したころに軽快傾向となり，退院時にはHb 10g/dl台まで改善した．

第2回入院までの経過：退院後は自宅で息子夫婦と同居し，近所に買い物に出かけて買い物ができるほどにADLは改善していた．貧血の進行も認めなかった．しかし，2003年1月頃から易疲労感を自覚し，2月頃から食欲低下が出現した．4月4日，38℃台に発熱したため当院救急外来を受診し，当科緊急入院となった．

入院時現症：身長148cm，体重37.2kg．体温38.4℃，

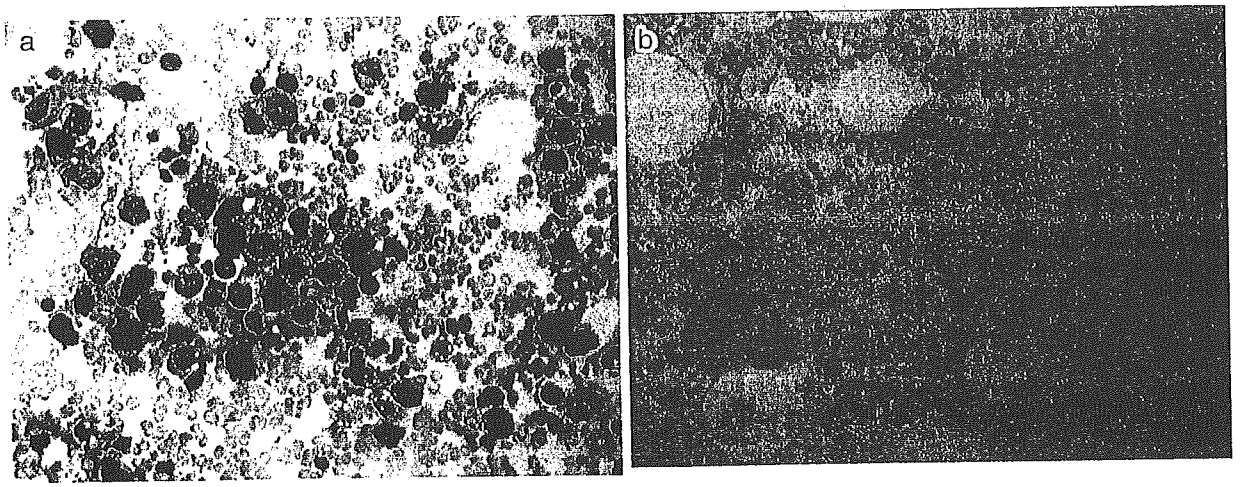

Fig. 3　第2回入院時に施行した骨髄穿刺標本
a　May-Giemza染色（×400）．大型の核と好酸性の大きな胞体を持つ，大型の異型細胞がびまん性に浸潤している．胞体内に空泡形成が認められ，一見“Starry-sky”様である．免疫組織学的にCD10陰性であった．
b　CD20免疫組織染色（×400）．CD20陽性細胞が褐色に染まる．

血圧90/60mmHg，脈拍86/分　整．意識レベルJapan Coma Scaleで I-1．長谷川式簡易知能評価スケール(HDS-R)は30点中12点．皮膚の弾性は低下しており，眼瞼結膜は貧血様．心尖部にLevine III/VIの収縮期雑音を聴取．脾臓を左肋弓下に2横指触知．表在リンパ節の腫脹なし．下腿浮腫なし．神経学的には四肢深部腱反射の減弱が認められた．

入院時検査所見：第2回入院時の検査所見をTable 2に示す．前回入院時と同様の汎血球減少と異型リンパ球の出現，LDH上昇，CRPやフェリチンの高値が認められた．また，可溶性IL-2レセプターの値は今回も高値(1,877U/ml）であった．

入院後の経過：第2回入院後の経過をFig. 1に示す．入院後施行した胸腹部造影CTでは，前回入院時には認めなかった脾臓の低吸収域が認められ，またガリウムシンチでも脾臓への取りこみが相対的に増加していた(Fig. 2)．さらに，骨髄穿刺標本において，大きな核と好酸性の大きな胞体を持つ，大型の異型細胞がびまん性に浸潤しており（Fig. 3a)，免疫組織学的にCD20陽性(Fig. 3b)，CD3，CD5，CD10は陰性，EBER（EBV-encoded RNAs)，LMP1(EBV-encoded latent protein 1)，EBNA2いずれも陰性であった．c-Myc遺伝子の転座(t(8；14)，t(8；2)，t(8；22))は認められなかった．以上から，びまん性大細胞型B細胞リンパ腫(diffuse large B-cell lymphoma：DLBCL）と診断した．

入院時より認めていた弛張熱は抗生剤に反応することなく，DLBCLと診断後に開始した化学療法（CHOP療法；cyclophosphamide，doxorubicin，vincristine，prednisolone）に速やかに反応し，解熱した（Fig. 1)．1コースの化学療法により症状は安定し，外来で化学療法を継続する方針となり，5月30日に退院となった．

考　察

本症例は古典的な不明熱の定義[1]を満足し，精査を行ったにもかかわらず当初は確定診断に至らず，約1年の経過で悪性リンパ腫との診断に至った．不明熱の原因疾患としては，今日においても①感染症，②悪性腫瘍，③血管炎症候群を含む膠原病，が大部分を占め，高齢者においてもこれら3つの病態が重要である[2]．

本症例の経過を解釈するにあたり問題となるのは，第1回目の入院時すでに悪性リンパ腫が潜在していたかどうかという点である．確かに，胆嚢穿刺で軽快した点や著明な弛張熱を示した臨床経過は悪性リンパ腫の経過と解釈するには十分とは言えない．しかし，第1回入院時に認められた汎血球減少，脾腫，異型リンパ球の存在，可溶性IL-2レセプターの異常高値のすべてを一元的に説明するためには感染症の存在のみでは説明が困難で，この時期に悪性リンパ腫が潜在していたことは十分可能性がある．ただし，リンパ腫がDLBCLであったか，他のindolentなリンパ腫であったかは不明である．indolentなリンパ腫からaggressiveなリンパ腫へのtransformationの報告をみると，follicular lymphoma（FL）

は5年間に22%，10年間に31%がtransformationを来たし[3]，transformationまでの期間は平均約66カ月であると報告されている[4]．またsplenic marginal zone lymphoma（SMZL）では再発例の10～20%がtransformationを来たしており，それまでの期間は中間値として12～85カ月と報告されている[5]．したがって，第1回入院中にindolentの悪性リンパ腫が潜在するかどうかは組織学的に確認していないが，1年間の経過観察中にFLやSMZLなどindolentな悪性リンパ腫からaggressiveな悪性リンパ腫（DLBCL）にhigher-grade transformationを来たした可能性も考えられる．第1回入院中，診断確定のための脾摘を行うことも検討したが，患者の全身状態を考慮して施行しなかった．逆に，第1回目の入院経過は悪性リンパ腫のみでは説明しがたい．その理由として，上述のとおり胆嚢穿刺のみで発熱の軽快，CRPの低下が認められたこと，B症状が強く前面に出ているにもかかわらず，リンパ腫そのものの治療なしに一度は軽快していることが挙げられる．そのため，何らかのウイルス感染症が第1回入院前に存在し，それが軽快する間もなく入院後に発症した胆道感染症が経過を複雑にしていた可能性が高いと考えられる．ただし，悪性リンパ腫との関連が報告されているEBウイルスに関しては，第1回，第2回入院時の各種抗体価が既感染パターンであり，第2回入院時にEBウイルスDNAは検出されなかった．また，リンパ腫組織の免疫染色の結果はEBER，LMP1，EBNA2いずれも陰性であり，本症例のリンパ腫発症機転にEBウイルスが関与していたとの証明はできなかった．また，赤芽球癆との関連性が報告されているパルボウイルスB19についてもIgM抗体を測定したが，2度の入院いずれの経過においても陰性であった．

PRCAが非胸腺性のリンパ増殖性疾患に伴って生じることは稀である．慢性リンパ性白血病に赤芽球癆を合併したとの報告は比較的多く認められ，その機序として，腫瘍性IgG-FcR$^+$ T-Cell（Tγ細胞），あるいはサプレッサーT細胞による赤血球前駆細胞の抑制が関与しているとの報告[6)~9)]がこれまでになされている．しかし，悪性リンパ腫とPRCAの合併についての報告は稀である[10)~12)]．その機序としては慢性リンパ性白血病の場合と同様の推測がなされているほか，悪性リンパ腫の患者血清IgGがCFU-Eを抑制したり[13)]，患者単核細胞がCFU-Eコロニーの形成を抑制するため[14)]と考えられている．臨床的にも，治療により悪性リンパ腫が寛解するとPRCAも改善したとする報告が散見される[15)16)]．本症例で行った血液細胞表面マーカーに関する検討の結果は，第1回入院時はCD8陽性T細胞（サプレッサーT細胞）が圧倒的優位であり，このため赤血球前駆細胞の抑制が生じた結果，赤芽球癆を呈した可能性は十分に考えられる．ただし，第1回入院後2カ月で軽快傾向に転じ，以後第2回入院まで一貫して貧血の進行を認めなかったことから，赤芽球癆の発症原因を悪性リンパ腫のみに求めることには無理がある．やはり第1回入院前から何らかの感染症が存在していたために赤芽球癆を発症したとするのが妥当であるが，上述の理由で，悪性リンパ腫が潜在していたことがこの経過を修飾した可能性は否定できない．

以上の考察から，本症例は以下のようにまとめることができる．本症例の不明熱の主因は，第1回目の入院の時点では何らかの感染症と考えられ，入院後に追って発症した感染症，とくに胆道感染が経過を修飾していたものと考えられる．しかし，悪性リンパ腫が潜在していた可能性は考慮しなければならない．その場合，CD8陽性T細胞によって赤血球前駆細胞が抑制されていたとすれば，これが赤芽球癆発症の経過に影響を与えていた可能性も推測される．その後1年の経過で高悪性度の悪性リンパ腫が顕在化し，その結果再び不明熱を呈し，第2回入院中に施行した骨髄穿刺の結果，DLBCLの診断に至った．

以上，原因不明の発熱で発症し，赤芽球癆が先行した高齢者悪性リンパ腫の一症例を報告した．高齢者は典型的な症状を示しにくく，また易感染性で悪性腫瘍の頻度も成人と比較して高率である．したがって，発熱のみを主症状とする節外性の悪性リンパ腫の場合には，他の疾患との鑑別がきわめて困難となる．B症状の頻度やperformance statusの程度も成人と差がないとする報告が多い．診断のための検査も不十分なものになりがちである．高齢者の不明熱においては血液悪性腫瘍，とくに悪性リンパ腫が潜在している可能性を念頭におき，精査を行うことが必要と考えられる．

なお，本論文の要旨は第39回日本老年医学会関東甲信越地方会（2004年3月，東京）において発表した．

謝辞：本症例の経過を考察するにあたり，貴重なご意見，ご指導をいただいた東京大学大学院医学系研究科血液腫瘍病態学講師　本倉　徹先生，同助手　伊豆津　宏二先生に深謝いたします．

文　献

1) Petersdorf RG, Beeson PB : Fever of unexplained origin : Report on 100 cases. Medicine 1961 ; 40 : 1—30.
2) Iikuni Y, Okada J, Kondo H, Kashiwazaki S : Current fever of unknown origin 1982-1992. Intern Med 1994 ; 33 :

67—73.
3) Bastion Y, Sebban C, Berger F, Felman P, Salles G, Dumontet C, et al.: Incidence, predictive factors, and outcome of lymphoma transformation in follicular lymphoma patients. J Clin Oncol 1997; 15: 1587—1594.
4) Yuen AR, Kamel OW, Halpern J, Horning SJ: Long-term survival after histologic transformation of low-grade follicular lymphoma. J Clin Oncol 1995; 13: 1726—1733.
5) Thieblemont C, Felman P, Callet-Bauchu E, Traverse-Glehen A, Salles G, Berger F, et al.: Splenic marginal-zone lymphoma: a distinct clinical and pathological entity. Lancet Oncol 2003; 4: 95—103.
6) Hoffman R, Kopel S, Hsu SD, Dainiak N, Zanjani ED: T cell chronic lymphocytic leukemia: presence in bone marrow and peripheral blood of cells that suppress erythropoiesis in vitro. Blood 1978; 52: 255—260.
7) Nagasawa T, Abe T, Nakagawa T: Pure red cell aplasia and hypogammaglobulinemia associated with Tγ-cell chronic lymphocytic leukemia. Blood 1981; 57: 1025—1031.
8) Mangan KF, Chikkappa G, Farley PC: T gamma (Tγ) cells suppress growth of erythroid colony-forming units in vitro in pure red cell aplasia of B-cell chronic lymphocytic leukemia. J Clin Invest 1982; 70: 1148—1156.
9) Mangan KF, D' Alessandro L: Hypoplastic anemia in B cell chronic lymphocytic leukemia: evolution of T cell-mediated suppression of erythropoiesis in early-stage and late-stage disease. Blood 1985; 66: 533—541.
10) Singh VP, Khanna A, Rai M, Sundar S, Shukla PK, Naresh T, et al.: Non-Hodgkin's lymphoma with pure red cell aplasia. J Assoc Physicians India 2001; 49: 1123—1124.
11) Katayama H, Takeuchi M, Yoshino T, Munemasa M, Tada A, Soda R, et al.: Epstein-Barr virus associated diffuse large B-cell lymphoma complicated by autoimmune hemolytic anemia and pure red cell aplasia. Leuk Lymphoma 2001; 42: 539—542.
12) Cobcroft R: Pure red cell aplasia associated with small lymphocytic lymphoma. Br J Haematol 2001; 113: 260.
13) 広沢信作，神山隆一，壇　和夫，厨信一郎，野村武夫：赤芽球癆を合併した悪性リンパ腫の1例．臨床血液 1982; 23: 1463—1467.
14) 片平潤一，高橋正知，溝口秀昭，森　茂郎，坂本保己：赤芽球癆を合併したB細胞性悪性リンパ腫における末梢単核細胞のCFU-E抑制作用．臨床血液 1986; 27: 496—500.
15) Carloss HW, Saab GA, Tavassoli M: Pure red cell aplasia and lymphoma. JAMA 1979; 242: 67—68.
16) Morgan E, Pang KM, Goldwasser E: Hodgkin disease and red cell aplasea. Am J Hematol 1978; 5: 71—75.

Abstract

Malignant lymphoma manifested by fever of unexplained origin and pure red cell aplasia in an elderly patient

Yoko Hanaoka, Hiroshi Yamamoto, Katsuya Iijima, Eijiro Ohga, Koichi Kozaki and Yasuyoshi Ouchi

A 76-year-old woman was admitted to the University of Tokyo Hospital in June 2002 because of fever of unexplained origin. She had suffered a high grade fever (above 39℃) for 2 weeks. Initial evaluation revealed elevated CRP and pancytopenia. Bone marrow aspiration (BMA) was performed, and a diagnosis of pure red cell aplasia (PRCA) was made. One month later, she complained right hypochondrial pain, and aspiration from her enlarged gall bladder was performed. Her fever and PRCA ameliorated, and she was discharged in August, 2002. In April 2003, she was readmitted to our hospital because of the recurrence of high grade fever, elevation of CRP, and pancytopenia. BMA was performed and revealed diffuse large B cell lymphoma. In the case of extranodal lymphoma which only presents pyrexia, differentiation with other diseases is very difficult especially in the elderly. It is necessary to bear in mind the possibility that a hematological malignancy, especially malignant lymphoma, can be latent in elderly patient with fever of unknown origin.

Key words: *Pure red cell aplasia, Fever of unexplained origin, Malignant lymphoma, Elderly*
(Jpn J Geriat 2005; 42: 444—449)

Department of Geriatric Medicine, the University of Tokyo Hospital

Computerized detection of intracranial aneurysms for three-dimensional MR angiography: Feature extraction of small protrusions based on a shape-based difference image technique

Hidetaka Arimura[a)]
Department of Health Sciences, School of Medicine, Kyushu University, 3-1-1, Maidashi, Higashi-ku, Fukuoka 812-8582, Japan

Qiang Li
Department of Radiology, The University of Chicago, 5841 South Maryland Avenue, Chicago, Illinois 60637

Yukunori Korogi
Department of Radiology, University of Occupational & Environmental Health School of Medicine, Kitakyushu 807-8555, Japan

Toshinori Hirai, Shigehiko Katsuragawa, and Yasuyuki Yamashita
Department of Radiology, Kumamoto University, Kumamoto 860-8556, Japan

Kazuhiro Tsuchiya
Department of Radiology, Kyorin University, Mitaka 181-8611, Japan

Kunio Doi
Department of Radiology, The University of Chicago, 5841 South Maryland Avenue, Chicago, Illinois 60637

(Received 2 August 2005; accepted for publication 6 December 2005; published 24 January 2006)

We have improved a computerized scheme for the detection of intracranial aneurysms for three-dimensional (3-D) magnetic resonance angiography (MRA) by the use of image features of small protrusions extracted based on a shape-based difference image (SBDI) technique. Initial candidates were identified by use of a multiple gray-level thresholding technique in dot enhanced images, and by finding short branches in skeleton images. Image features related to aneurysms were determined based on candidate regions segmented by use of a region growing technique. For extracting additional features on small protrusions or small aneurysms, we have developed an SBDI technique, which was based on the shape-based difference between an original segmented vessel and a vessel with suppressed local change in thickness. The SBDI technique was useful for obtaining local changes in vessel thickness, i.e., SBD regions, which could be small aneurysms in the case of true positives, but thin or very small regions in the case of false positives. Many false positives were removed by means of rule-based schemes and linear discriminant analysis on various 3-D localized image features, including SBDI features. We tested the computerized scheme on 53 cases with 61 aneurysms and 62 nonaneurysm cases based on a leave-one-out-by-patient test method. As a result, false positives per patient decreased from 5.8 to 3.8, while a high sensitivity of 97% was maintained by use of the SBDI technique, in which SBDI features were effective for removing some false positives. The computer-aided diagnostic (CAD) scheme may be robust and useful in assisting radiologists in the detection of intracranial aneurysms for MRA. © *2006 American Association of Physicists in Medicine.* [DOI: 10.1118/1.2163389]

Key words: shape-based difference image technique, computer-aided diagnosis (CAD), intracranial aneurysms, magnetic resonance angiography (MRA)

I. INTRODUCTION

Subarachnoid hemorrhage (SAH) due to ruptures of intracranial aneurysms kills 10 000 persons each year in North America.[1] SAH is a serious disorder with high mortality and morbidity, accounting for about one-quarter of cerebrovascular deaths. From 3.6% to 6% of the adult population have intracranial aneurysms, which may rupture at an annual rate of 1% to 2%.[2,3] Magnetic resonance angiography (MRA) can be used to screen noninvasively for intracranial aneurysms in asymptomatic patients who have a family history of aneurysms or who have polycystic kidneys, coarctation of the aorta, or collagen vascular disease, putting them at an increased risk for aneurysms. In these patients, it is very important to detect unruptured aneurysms as early as possible and to treat or follow up the aneurysms. However, it is difficult and time consuming for radiologists to detect small aneurysms, and it may not be easy to find even medium-sized aneurysms because of their overlap with adjacent vessels or because of unusual locations in maximum intensity projection (MIP) images of MRA. For correct and efficient detection of intracranial aneurysms with MRA, therefore, radiologists would need a number of training sessions.

Since the mid-1980s, a number of researchers have developed computer-aided diagnostic (CAD) schemes for detection and classification of various kinds of abnormalities such as microcalcifications and masses in mammograms,[4,5] pulmonary nodules and diffuse lung diseases in CT,[6–8] and colonic polyps in CT colonography.[9,10] Besides, the clinical usefulness of CAD schemes has been studied.[11] In the detection of intracranial aneurysms by MRA, CAD schemes would be useful in assisting radiologists. Therefore, we developed a computerized scheme for automated detection of unruptured intracranial aneurysms in MRA based on the use of a three-dimensional (3-D) selective enhancement filter for dots (aneurysms).[12,13] Twenty-nine cases with 36 unruptured aneurysms (diameter: 3–26 mm, mean of 6.6 mm) and 31 nonaneurysm cases were tested. The CAD scheme correctly detected all of 36 aneurysms with 2.4 false positives per patient based on a leave-one-out-by-patient test method. However, for a large database (53 cases with 61 aneurysms and 62 nonaneurysm cases), the previous scheme[12] above produced 5.8 false positives per patient at a sensitivity of 97%. As a result of investigation on the false positives, we found that about 65% of the false positives were of the single-vessel type and the bifurcation type. Therefore, in this study, we focused on removing these two types of false positives.

Our purpose of this study was to improve the CAD scheme for the automated detection of unruptured intracranial aneurysms in MRA by use of image features of small protrusions extracted based on a shape-based difference image (SBDI) technique. The SBDI technique was based on the shape-based difference between an original segmented vessel and a vessel with suppressed local changes in thickness. The performance of our CAD scheme was evaluated by the use of 115 cases (53 cases with 61 aneurysms and 62 nonaneurysm cases) based on a free-response receiver operating characteristic (FROC) curve. For an estimation of the robustness of our scheme, we tested it for an independent set of 63 cases (34 cases with 36 aneurysms and 29 nonaneurysm cases) acquired from a different MRI at a different institution.

II. METHODS AND MATERIALS

A. Overall scheme

Figure 1 shows the overall scheme developed in this study, where a feature extraction procedure based on the SBDI technique was incorporated into the previous scheme.[12] Our approach for the identification of initial candidates was based not only on enhancement of aneurysms by use of a selective enhancement filter for dots (aneurysms),[14] but also on finding short branches on parent skeletons in skeleton images, which can indicate the high likelihoods of small aneurysms.[12] The image features of aneurysm candidates were determined based on candidate regions segmented by the use of a region growing technique. In addition to these features, in this study, useful image features related to small protrusions were extracted from the SBD regions (obtained by the SBDI technique), which could be small aneurysms for true positives, but thin or very small regions for false positives. Finally, false positives were removed by use of rule-based schemes and linear discriminant analysis (LDA).

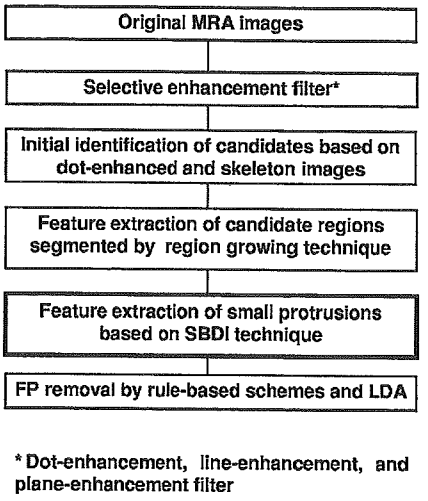

FIG. 1. Overall CAD scheme for detection of intracranial aneurysms at 3-D MRA.

B. Initial identification of aneurysm candidates based on dot-enhanced image and skeleton image

The selective enhancement filters for dots,[14] which can enhance dot-like objects, were applied to isotropic 3-D MRA images. Figure 2 shows an original MRA image with a large aneurysm within a search region, and its dot-enhanced image, where the aneurysm was enhanced well. For avoiding picking up a number of regions irrelevant to vessels, the search region was determined for identifying initial candidates by dilation of major vessels segmented in an MRA image.[15] The initial candidates were identified with a multiple-gray-level thresholding technique for finding local peaks of voxel values in 3-D dot-enhanced images within the search region, and the candidate regions were segmented by the use of a region growing technique.[12] However, some

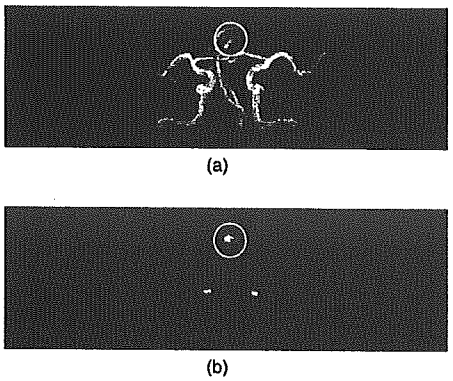

FIG. 2. An illustration of (a) an original MRA image and (b) its corresponding dot-enhanced image, all of which were produced by MIP image processing. Circles indicate a large aneurysm with a diameter of 10.0 mm on the top of the basilar artery.

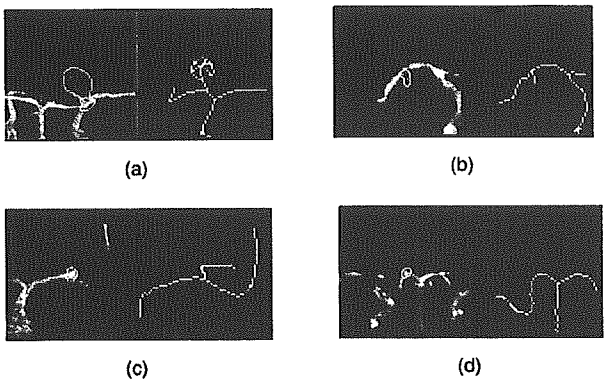

FIG. 3. Illustration of four types of aneurysms in original images with segmented regions (white lines) and the corresponding skeleton images. (a) Large type, (b) short-branch type, (c) bifurcation type, and (d) single-vessel type.

small aneurysms adjacent to a bending region of a thick vessel were not enhanced well by the dot enhancement filter, because the bending region was strongly enhanced. In that case, the bending region was picked up as an "aneurysm" candidate instead of the true aneurysm. However, we found that such small aneurysms became a short branch on the parent vessel in the skeleton image. Therefore, if the short branch was detected in a spherical area adjacent to the original candidate region (e.g., bending region) in a skeleton image, the short branch was considered to be an additional candidate of the short branch type and was segmented based on a region-growing technique.

C. Feature extraction of candidate regions segmented by a region growing technique

Image features of candidates were determined based on the regions segmented by use of a region growing technique in the dot-enhanced images and original images. Our segmentation method was based on finding a large change in some image features, which implied that the candidate region merged with its adjacent background or other candidates, as the candidate region grew.[12] All candidates were classified into four categories based on the effective diameter and local structures determined from the skeleton image, i.e., large type, short-branch type, bifurcation type, and single-vessel type, as shown in Fig. 3, because the image features of aneurysms and false positives in each category differed from each other. Short-branch-type candidates were segmented based on region growing in the original image from the short branch as a seed region. For segmented regions of aneurysm candidates, gray-level features and morphological features as shown in Table I were determined in the original images, dot-enhanced images, line-enhanced images, plane-enhanced images, distance-transformed images, and skeleton images; the definitions of image features are described in the Appendix.

For large aneurysm candidates, image features relevant to the characteristics of large aneurysms were determined, i.e., the average voxel value and the standard deviation (SD) of the voxel value in the core and rind regions of the segmented candidates in the original images, because the characteristics of the large aneurysms were different from those of small aneurysms.[12] In addition, specific features for the short-branch-type candidates were determined, i.e., the protrusion length and the average distance value in the candidate region obtained from the distance-transformed image.

D. Shape-based difference image (SBDI) technique

The SBDI technique was developed for the extraction of local changes in vessel thickness based on distance-transformed images and skeleton images. The local changes in the thickness could be caused by aneurysms, stenosis, etc. The overall algorithm of the SBDI technique is shown in Fig. 4. A vessel with a candidate was segmented within a volume of interest by use of a segmentation method (e.g., a region growing technique as used in this study). The SBDI technique is based on the shape-based difference (SBD region) between an original segmented vessel and a vessel with suppressed local change in thickness by use of logical Exclusive OR (XOR) operation. In this study, SBD regions were ex-

TABLE I. Gray-level features and morphological features used in this study.

Gray level features:
Average voxel value
Standard deviation (SD) of voxel value
Relative contrast to average voxel value
Relative difference is SD of voxel values between inside and outside regions
Relative difference in average voxel values between inside and outside regions
Morphological features:
Effective diameter
Sphericity
Relative SD of the distance between centroid and surface
Maximum and minimum distance between centroid and surface
Difference between maximum and minimum distance betweeen centroid and surface
Maximum or average distance value of distance-transformed image
Relative difference in maximum distance between inside and outside regions
Length of protrusion

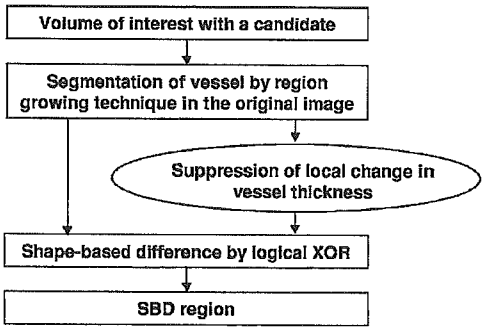

FIG. 4. Overall algorithm of a shape-based difference image (SBDI) technique.

tracted as "small protrusions" or "small aneurysms" from parent vessels, and SBD image features were calculated.

Figure 5 shows the algorithm for deriving the vessel with suppressed local changes in thickness. Distance transformed images were obtained from the segmented vessels, and then the skeleton images with distance values, i.e., vessel thickness, were determined by logical AND operation between the skeleton image and the distance-transformed image.[16,17] By use of a reverse distance transformation of the skeleton image with distance values, the original segmented vessel can be recovered.[18] However, if the local changes in vessel thickness caused by aneurysms are suppressed by smoothing of the skeleton image with a rind filter, a vessel with suppressed local changes in thickness was produced instead of the original vessel. The rind filter was a hollow-sphere filter with a one-voxel rind, where the rind region had a value of one and the inside region had a value of zero. By use of the rind filter, the voxel value at the center of the sphere was replaced by the maximum distance value within the rind region. The diameter of the rind filter was determined to be three times larger than the maximum distance value on the skeleton image within the candidate region.

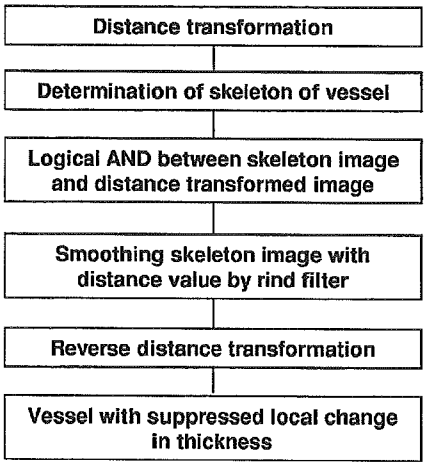

FIG. 5. Algorithm for deriving the vessel with suppressed local change in vessel thickness.

E. Feature extraction of small protrusion based on SBDI technique

The SBDI technique is used for extracting useful image features from SBD regions, which could be small aneurysm regions for true positives, but thin or very small regions for false positives. The thickness of a vessel with a small aneurysm could be larger in the aneurysm region than in other regions, and thus an extracted SBD region would be a small aneurysm region, and the sphericity of the SBD region could be relatively high. On the other hand, in a vessel without an aneurysm, which is a false positive in this study, the local change in vessel thickness would be very small. As a result, the SBD region could be a thin or very small region, and thus the sphericities of the SBD regions obtained from the false positives could be smaller than those of aneurysms. Therefore, it is possible to remove some false positives among aneurysm candidates by using image features extracted from SBD regions. From the SBD regions and original images, we determined seven image features, i.e., effective diameter, sphericity, relative SD of the distance value between centroid and surface, maximum and minimum distance value between centroid and surface, contrast, average voxel value, and SD of the voxel value, which were used for rule-based schemes and LDA.

However, because the large type and short branch type of aneurysms are branches from a parent vessel on the skeleton image, as shown in Fig. 3, there were small local changes in the thicknesses of parent vessels. Therefore, we applied the SBDI technique only to the single-vessel type and bifurcation type.

F. False positive removal based on rule-based schemes and LDA

For the removal of false positives, all rules used in rule-based schemes were automatically determined based on image features of all training aneurysms in each category (Fig. 3) by the use of simple thresholdings, such as 5% higher and 5% lower than the maximum and minimum values of each feature.

The LDA was applied for the further removal of false positives. The LDA is one of multivariate analysis methods. The basic idea of the LDA is to discriminate between two groups based on an output of a linear discriminant function (LDF) derived from the data of two groups (e.g., Group A and B), and then to classify unknown data into one of the two groups. The unknown data is classified by thresholding the output of the LDF (e.g., if the output was plus, the unknown data would be determined to belong to a Group A). In this study, the LDF was derived from four image features (variables) of all cases except one case, and then all candidates in the case left out was classified with the LDF into aneurysm-candidate group and false-positive group.

The number of features for the short-branch-type candidates was limited, because the candidate regions were identified based on short branches in the skeleton images, not on the dot-enhanced image. Therefore, image features related to dot-enhanced images were not obtained for short-branch-

type candidates. Consequently, seven common features for short-branch-type candidates and for the other candidates can be used for the LDA. However, an effective image feature combination was chosen by use of a stepwise selection method based on Wilks' lambda and the Az value. Wilks' lambda is defined by the ratio of within-group variance to the total variance,[19] which indicates the degree of discrimination between true positives and false positives, and Az value is the area under the receiver operating characteristic (ROC) curve, which indicates an accuracy for detection of aneurysms. An initial combination of features was obtained in the stepwise method, and then an effective feature combination was selected from the initial combination of features based on the highest Az value. In the stepwise method, each feature was added or removed one by one by the use of two thresholds on the F value, one for removal and another for addition, by use of the F value, which is based on Wilks' lambda.[20] For this procedure, we employed 29 cases with 36 unruptured aneurysms and 31 nonaneurysm cases used in the previous study,[12] which was a part of Database A described in the next section. As a result, the final combination consisted of four features, i.e., the average voxel value, the relative SD of the voxel value, the relative SD of the distance between the centroid and the surface, and the difference between the maximum and minimum distance (between the centroid and the surface).

G. Subjects

We employed two databases obtained from different institutions, i.e., 53 cases with 61 aneurysms (diameter: 3–26 mm, mean of 6.6 mm) and 62 nonaneurysm cases obtained from a Siemens 1.5 T unit (Database A), and 34 cases with 36 aneurysms (1–15 mm, mean of 5.2 mm) and 29 nonaneurysm cases from a Toshiba 1.5 T unit (Database B). All aneurysms were diagnosed by digital subtraction angiography, computed tomographic angiography, surgery, or by MRA that was assessed by two experienced neuroradiologists.

Database A: MRA axial images with 512×512 pixels and a pixel size of 0.391 or 0.410 mm were acquired from 115 patients on a 1.5 T MRI scanner (Magnetom Vision, Siemens Medical Systems, Erlangen, Germany) by use of a 3-D time-of-flight (3D-TOF) technique in the Department of Radiology, Kumamoto University. The 3-D MRA images included 64, 96, or 128 slices with a slice thickness of 1.0, 0.67, or 0.5 mm, respectively. An isotropic 3-D image was $400 \times 400 \times 128$ voxels with a voxel size of 0.5 mm produced from the original 3-D MRA images by use of linear interpolation and/or cropping.

Database B: Sixty-three cases were acquired on a 1.5 T MRI scanner (Excelart, XG SPIN Edition, Toshiba Medical Systems, Tochigi, Japan) by means of a 3-D-TOF technique in the Department of Radiology, Kyorin University. Original 3-D MRA images with a pixel size of 0.3906 or 0.4167 mm and a slice thickness of 1.0 or 1.1 mm were converted into isotropic 3-D images with $400 \times 400 \times 120$–$160$ voxels and a voxel size of 0.5 mm by the use of linear interpolation and/or cropping.

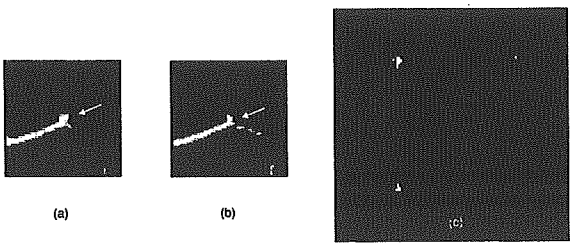

FIG. 6. An illustration of (a) an original segmented vessel with an aneurysm, (b) a vessel with a suppressed aneurysm, and (c) a cross section of an SBD region in coronal (top left), sagittal (top right), and axial (bottom left) planes.

H. Evaluation of the performance

The performance of our CAD scheme was evaluated for Database A based on a FROC curve, whereas the robustness of the scheme was estimated for the independent Database B. We tested our CAD scheme for the two databases separately with a leave-one-out-by-patient test method. Because each database was relatively small, we needed to use as many cases as possible for the robust training of the CAD scheme. However, if databases for testing were very large, a half-and-half split test or n-way cross-validation test would be more appropriate.

With this test method, all aneurysm candidates except those from one patient were used for training with two rule-based schemes and the linear discriminant function, and the candidates left out were used for testing. This procedure was repeated for all patients, so that all candidates in each patient were used once as test candidates. By changing a threshold value for discriminant scores of the candidates produced with the linear discriminant function, which was determined by LDA for distinction between aneurysms and false positives, we determined the FROC curve of the CAD scheme. For obtaining the FROC curve, we sequentially applied rule-based schemes and LDA to all candidates based on the leave-one-out-by-patient test method.

III. RESULTS AND DISCUSSION

The effects of the SBDI technique on a true positive and a false positive, i.e., the vessel with and without an aneurysm, are shown in Figs. 6 and 7, respectively. By use of the SBDI technique, the vessel with a suppressed local change in vessel thickness was derived, as shown in Fig. 6(b) from the original segmented vessels with an aneurysm (bifurcation type), as shown in Fig. 6(a). Although the thicknesses of some portions of the vessel changed from the original one, as shown in Fig. 6(b), an aneurysm was suppressed effectively. As a result, the SBD region was extracted from the parent vessel as an aneurysm region, as shown in Fig. 6(c). On the other hand, for the false positive in Fig. 7, the original vessel as shown in Fig. 7(a) was similar to the vessel with suppressed local change in vessel thickness as shown in Fig.

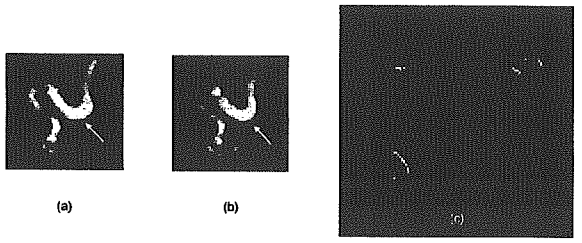

FIG. 7. An illustration of (a) an original segmented vessel without an aneurysm (false positive), (b) vessel with suppressed local change in vessel thickness, and (c) cross section of an SBD region in coronal (top left), sagittal (top right), and axial (bottom left) planes.

7(b), because the local changes in the vessel thickness without aneurysms were small. Consequently, the difference between the original and suppressed images, i.e., the SBD region, was very small, as shown in Fig. 7(c).

Figure 8 shows the relationship between the effective diameter and sphericity of candidates of the single vessel type for Database A. The sphericities of many false positives were smaller than those of aneurysms, because only thin rind regions or tiny regions could have remained for the false positives as SBD regions as shown in Fig. 7(c), whereas small protrusions with a semispherical shape would have been extracted for small aneurysms, as shown in Fig. 6(c). Furthermore, the effective diameters of some false positives were relatively smaller than those of many aneurysms, except one aneurysm. Therefore, many false positives can be eliminated by the use of some appropriate rules.

Figure 9 shows the FROC curve for the overall performance of our scheme for Database A by the use of LDA with the leave-one-out-by-patient test method. For producing the FROC curve with the SBDI technique, we applied our scheme to the candidates at an operating point without the SBDI technique, i.e., the sensitivity was 97% with 5.8 false positives per patient. As a result, our scheme achieved the

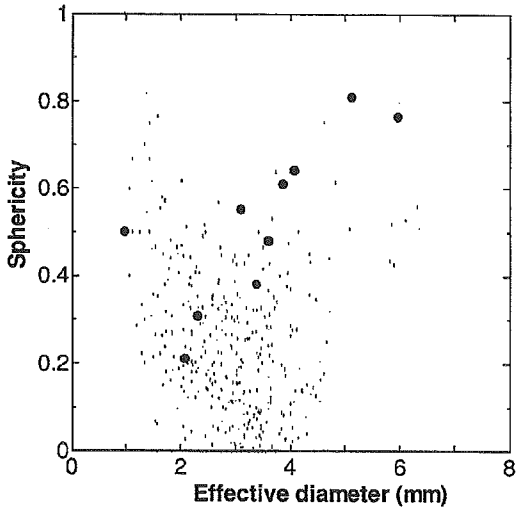

FIG. 8. The relationship between the effective diameter and sphericity of candidates of a single vessel type for Database A.

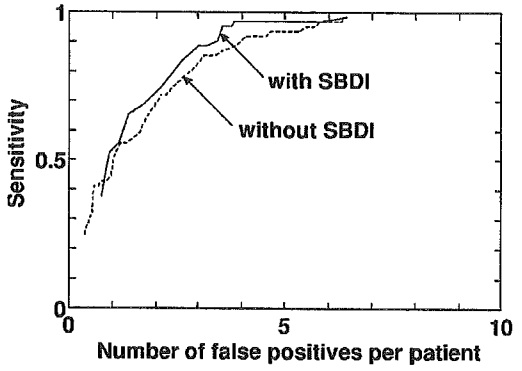

FIG. 9. FROC curve for the overall performance of our scheme for Database A by use of LDA with the leave-one-out-by-patient test method.

same sensitivity of 97% with 3.8 false positives per patient for 115 cases. The SBDI technique was applied to only the bifurcation type and single vessel type of candidates. The total number of the bifurcation type and single vessel type of false positives per patient decreased by 53% compared with the result without the SBDI technique. This result shows that the SBD image features would be effective for removing the bifurcation type and single-vessel type of false positives.

To evaluate the robustness of our scheme, we tested our scheme for an independent different database with different aneurysm sizes, i.e., Database B acquired from a Toshiba MRI scanner at Kyorin University. In the leave-one-out-by-patient method test, all rules for false positive removal were automatically determined from the image features of aneurysms included in Database B, but the other parameters of the scheme (e.g., the minimum effective diameter for initial candidates, thickness and diameter of the hollow rind filter) were the same as used for Database A. The image features on LDA were the same as used for Database A. As a result, the best performance of our CAD scheme for Database B indicated a sensitivity of 94% with 2.3 false positives per patient. This result may show that our scheme would be robust for a different database acquired by a different MRI scanner at a different institute if the rules for the CAD system would be retrained appropriately at each institution. We believe that most CAD systems would require retraining of rules for the detection of aneurysms in practical use at each institution, because the CAD performance varies depending on the image quality of MRA, which could differ by institution and MRI scanner. However, the method for retraining of the rules should be relatively simple or be automated, as described in Sec. II F. Nevertheless, for a further investigation of the robustness of our scheme, our CAD scheme needs to be applied to several independent databases acquired from different MRI scanners with different magnitudes of magnetic field at different institutions.

Undersampling for small aneurysms, i.e., larger slice thickness compared with small aneurysms, could affect the CAD performance. However, the slice thickness should be determined according to the minimum diameter of target aneurysms. In a previous study, we focused on aneurysms

equal to or larger than 3.0 mm, because the possibility of rupture for aneurysms smaller than 3.0 mm would be uncertain. However, for investigating the potential of our CAD scheme for very small aneurysms, in this study, we applied it to Database B, including ten aneurysms equal to or smaller than 2 mm, where two aneurysms were 1 mm and eight aneurysms were 2 mm. For detecting small aneurysms with 1 and 2 mm diameters, the sampling intervals should be smaller than 0.5 and 1 mm, respectively. However, the original slice thickness in the Database B was 1.0 or 1.1 mm, which was undersampling for such very small aneurysms, although the voxel size after linear interpolation was 0.5 mm. Nevertheless, the CAD scheme was able to detect one of two 1 mm aneurysms and seven of eight 2 mm aneurysms, and the sensitivity was 80% for such very small aneurysms. We believe that if the original slice thickness was smaller than 0.5 mm, the performance of our CAD scheme would be higher. Therefore, this result showed the potential of our CAD scheme for the detection of very small aneurysms.

In conclusion, we have improved a computerized scheme for the detection of intracranial aneurysms for 3-D MRA based on the SBDI technique. While keeping a high sensitivity of 97%, the number of false positives per patient decreased by 2.0 (from 5.8 to 3.8) by use of the SBDI technique. Our scheme may be robust and useful in assisting radiologists for detecting aneurysms at 3-D MRA for various aneurysm sizes and image qualities.

ACKNOWLEDGMENTS

The authors are grateful to Mitsue Miyazaki, Ph.D., Toshiba Corporation, for her useful discussion, and Ms. Elisabeth Lanzl for improving the manuscript. This work is supported in part by USPHS Grants No. CA 61625 and No. CA 98119. S. Katsuragawa and K. Doi are shareholders of R2 Technology, Inc., Los Altos, CA. CAD technologies developed in the Kurt Rossmann Laboratories have been licensed to companies including R2 Technology, Deus Technologies, Riverain Medical Group, Mitsubishi Space Software Co., Median Technologies, General Electric Corporation, and Toshiba Corporation. It is the policy of The University of Chicago that investigators disclose publicly actual or potential significant financial interests that may appear to affect research activities or that may benefit from research activities.

APPENDIX: DEFINITIONS OF IMAGE FEATURES SHOWN IN TABLE I

The image features shown in Table I are defined in this appendix.

Gray level features:

(1) Average voxel value: Average voxel value within a segmented region.
(2) Standard deviation (SD) of voxel value: SD of voxel value within a segmented region.
(3) Relative contrast to average voxel value: Difference between maximum and minimum voxel values divided by average voxel value within a segmented region.
(4) Relative difference in SD of voxel values between candidate and outside regions: Difference in SD of voxel values between candidate and outside regions divided by the SD within a candidate region. The candidate and outside regions for each candidate were defined by the candidate region at a current gray level threshold and the increased region at the subsequent gray level threshold in region growing technique, respectively.
(5) Relative difference in average voxel values between candidate and outside regions: Difference in average voxel values between candidate and outside regions divided by average voxel value within a candidate region.

Morphological features:

(1) Effective diameter: Diameter of a sphere with the same volume as that of the candidate.
(2) Sphericity: Fraction of the overlap volume between the candidate region and the sphere with the same volume as the candidate volume.
(3) Relative SD of the distance between centroid and surface: SD of Euclidean distance value between centroid and surface voxels in terms of candidate region divided by average distance value.
(4) Maximum and minimum distance between centroid and surface: Maximum and minimum Euclidean distance between centroid and surface voxels.
(5) Difference between maximum and minimum distance between centroid and surface: Difference between maximum and minimum Euclidean distance between centroid and surface voxels.
(6) Maximum or average distance value of distance-transformed image: Maximum or average distance value of distance-transformed image derived from a segmented region with a candidate in the original image.
(7) Relative difference in maximum distance between candidate and outside regions: Difference in maximum distance value of distance-transformed image between candidate and outside regions divided by the maximum distance within the candidate region.
(8) Length of protrusion: Difference between the short-branch length in the skeleton image and the radius of a parent vessel obtained from the distance-transformed image.

[a]Address correspondence to: Hidetaka Arimura, Ph.D., Department of Health Sciences, School of Medicine, Kyushu University, 3-1-1, Maidashi, Higashi-ku, Fukuoka 812-8582, Japan. Electronic mail: arimura@shs.kyushu-u.ac.jp

[1]J. T. King Jr., "Epidemiology of aneurysm subarachnoid hemorrhage," Neuroimaging Clin. N. Am. **7**, 659–668 (1997).
[2]J. M. Wardlaw and P. M. White, "The detection and management of unruptured intracranial aneurysms," Brain **123**, 205–221 (2000).
[3]S. Juvela, M. Porras, and K. Poussa, "Natural history of unruptured intracranial aneurysms: probability of and risk factors for aneurysm rupture," J. Neurosurg. **93**, 379–87 (2000).

[4]H. P. Chan, K. Doi, C. J. Vyborny, R. A. Schmidt, C. E. Metz, K. L. Lam, T. Ogura, Y. Wu, H. MacMahon, and E. A. Sickles, "Improvement in radiologists' detection of clustered microcalcifications on mammograms—The potential of computer-aided diagnosis," Invest. Radiol. **25**, 1102–1110 (1990).
[5]Z. Huo, M. L. Giger, C. J. Vyborny, and C. E. Metz, "Effectiveness of CAD in the diagnosis of breast cancer: An observer study on an independent database of mammograms," Radiology **224**, 560–568 (2002).
[6]H. Arimura, S. Katsuragawa, K. Suzuki, F. Li, J. Shiraishi, and K. Doi, "Computerized scheme for automated detection of lung nodules in low-dose CT images for lung cancer screening," Acad. Radiol. **11**, 617–629 (2004).
[7]Y. Uchiyama, S. Katsuragawa, H. Abe, J. Shiraishi, F. Li, Q. Li, C.-T. Zhang, K. Suzuki, and K. Doi, "Quantitative computerized analysis of diffuse lung disease in high-resolution computed tomography," Med. Phys. **30**, 2440–2464 (2003).
[8]F. Li, H. Arimura, K. Suzuki, J. Shiraishi, Q. Li, H. Abe, R. Engelmann, S. Sone, H. MacMahon, and K. Doi, "Computer-aided detection of peripheral lung cancers missed at CT: ROC analyses without and with localization," Radiology **237**, 684–690 (2005).
[9]H. Yoshida, Y. Masutani, P. MacEneaney, D. Rubin, and A. H. Dachman, "Computerized detection of polyps in CT colonography," Radiology **222**, 327–336 (2002).
[10]J. Nappi and H. Yoshida, "Feature-guided analysis for reduction of false positives in CAD of polyps for CT colonography," Med. Phys. **30**, 1592–1601 (2003).
[11]K. Doi, "Current status and future potential of computer-aided diagnosis in medical imaging," Br. J. Radiol. **78**, S3–S19 (2005).
[12]H. Arimura, Q. Li, Y. Korogi, T. Hirai, H. Abe, Y. Yamashita, S. Katsuragawa, R. Ikeda, and K. Doi, "Automated computerized scheme for detection of unruptured intracranial aneurysms in three-dimensional MRA," Acad. Radiol. **11**, 1093–1104 (2004).
[13]T. Hirai, Y. Korogi, H. Arimura, S. Katsuragawa, M. Kitajima, M. Yamura, Y. Yamashita, and K. Doi, "Intracranial aneurysms at MR angiography: Effect of computer-aided diagnosis on radiologists' detection performance," Radiology **237**, 605–610 (2005).
[14]Q. Li, S. Sone, and K. Doi, "Selective enhancement filters for nodules, vessels, and airway wall in two- and three-dimensional CT scans," Med. Phys. **30**, 2040–2051 (2003).
[15]H. Arimura, Q. Li, Y. Korogi, T. Hirai, H. Abe, Y. Yamashita, S. Katsuragawa, R. Ikeda, and K. Doi, "Development of CAD scheme for automated detection of intracranial aneurysms in magnetic resonance angiography," *18th International Congress of CARS—Computer Assisted Radiology and Surgery*, Chicago, USA, ICS, 2004, Vol. 1268, pp. 1015–1020.
[16]T. Saito and J. Toriwaki, "New algorithms for Euclidean distance transformations of an n-dimensional digitized picture with applications," Pattern Recogn. **27**, 1551–1565 (1994).
[17]T. Saito and J. Toriwaki, "A sequential thinning algorithm for three dimensional digital pictures using the Euclidean distance transformation," *Proc. 9th Scandinavian Conf. Image Analysis*, SCIA'95, 1995, pp. 507–516.
[18]G. Borgefors, K. I. Nystro, and G. S. D. Baja, "Computing skeletons in three dimensions," Pattern Recogn. **32**, 1225–1236 (1999).
[19]R. A. Johnson and D. W. Wichern, *Applied Multivariate Statistical Analysis* (Prentice-Hall, Englewood Cliffs, NJ, 1992), Sec. 5.3, pp. 184–188.
[20]M. Aoyama, Q. Li, S. Katsuragawa, H. MacMahon, and K. Doi, "Automated computerized scheme for distinction between benign and malignant solitary pulmonary nodules on chest images," Med. Phys. **29**, 701–708 (2002).

Radiology

Toshinori Hirai, MD
Yukunori Korogi, MD
Hidetaka Arimura, PhD
Shigehiko Katsuragawa, PhD
Mika Kitajima, MD
Masayuki Yamura, MD
Yasuyuki Yamashita, MD
Kunio Doi, PhD

Published online before print
10.1148/radiol.2372041734
Radiology 2005; 237:605–610

Abbreviations:
A_z = area under receiver operating characteristic curve
CAD = computer-aided detection
MIP = maximum intensity projection

[1] From the Department of Diagnostic Radiology, Graduate School of Medical Sciences, Kumamoto University 1-1-1 Honjo, Kumamoto 860-8556, Japan (T.H., S.K., M.K., M.Y., Y.Y.); Department of Radiology, University of Occupational and Environmental Health, School of Medicine, Kitakyushu, Japan (Y.K.); Department of Health Sciences, Kyushu University, Fukuoka, Japan (H.A.); and Department of Radiology, University of Chicago, Chicago, Ill (K.D.). Received October 9, 2004; revision requested December 20; revision received January 6, 2005; accepted January 25. **Address correspondence to** T.H. (e-mail: *toshinor@beige.ocn.ne.jp*).

Authors stated no financial relationship to disclose.

Author contributions:
Guarantors of integrity of entire study, T.H., Y.K., H.A., S.K., K.D.; study concepts/study design or data acquisition or data analysis/interpretation, all authors; manuscript drafting or manuscript revision for important intellectual content, all authors; approval of final version of submitted manuscript, all authors; literature research, T.H.; clinical studies, H.A., S.K., M.K., M.Y.; statistical analysis, T.H., S.K.; and manuscript editing, T.H., Y.K., H.A., S.K., Y.Y., K.D.

Intracranial Aneurysms at MR Angiography: Effect of Computer-aided Diagnosis on Radiologists' Detection Performance[1]

PURPOSE: To retrospectively evaluate the effect of computer-aided detection (CAD) on radiologists' performance in detection of intracranial aneurysms with magnetic resonance (MR) angiography.

MATERIALS AND METHODS: The institutional review board approved this study and did not require patient informed consent. Fifty maximum intensity projection MR angiograms in 50 patients were used for observer performance study. The group included 22 patients (age range, 43–86 years; mean, 60.2 years; 6 men and 16 women) with intracranial aneurysms and 28 patients (age range, 32–80 years; mean, 58.8 years; 10 men and 18 women) without aneurysms. The MR angiograms were obtained with three-dimensional time-of-flight 1.5-T MR imaging. Fifteen radiologists, including eight neuroradiologists and seven general radiologists, participated in the observer performance test. They interpreted the angiograms first without and then with the aid of the computer output by using an automated computerized scheme. The observers' performance without and with the computer output was evaluated with receiver operating characteristic analysis.

RESULTS: For all 15 observers, average area under the receiver operating characteristic curve (A_z) value for detection of aneurysms was increased significantly from 0.931 to 0.983 (P = .001) when they used the computer output. A_z values for general radiologists and neuroradiologists increased from 0.894 to 0.983 (P = .022) and from 0.963 to 0.984 (P = .014), respectively. Improvement in the performance of general radiologists in terms of the A_z value was much greater than that of neuroradiologists. Performance of general radiologists with CAD (A_z = 0.983) slightly exceeded that of neuroradiologists without CAD (A_z = 0.963) (P = .048).

CONCLUSION: CAD improved neuroradiologists' and general radiologists' performance for detection of intracranial aneurysms with MR angiography; improvement was greater for general radiologists than it was for neuroradiologists.

The natural history of unruptured intracranial aneurysms is not completely understood. Findings at autopsy and angiographic studies showed that between 3.6% and 6% of the general population harbor an unruptured intracranial aneurysm (1). The analytic results of the International Study of Unruptured Intracranial Aneurysms indicated that the risk of rupture is related to the site and size of an aneurysm and to a history of subarachnoid hemorrhage (2). With regard to treatment for unruptured intracranial aneurysms, benefits of surgical treatment or of endovascular intervention have been suggested in some studies (3,4). Recently, the investigators of the International Study of Unruptured Intracranial Aneurysms proposed that the specific risks related to the natural history of intracranial aneurysms should be considered in the treatment of each patient (5).

Magnetic resonance (MR) angiography is a widely available and noninvasive imaging modality that has high sensitivity for the detection of intracranial aneurysms. The accuracy of MR angiography in the detection of intracranial aneurysms is about 90% (6). The sensitivity of MR angiography was greater for detection of aneurysms larger than 3 mm than it was for detection of aneurysms that were 3 mm or smaller, that is, 94% versus 38% (6).

During the past 10 years, screening of unruptured intracranial aneurysms with MR angiography has gained attention, for example, for examining asymptomatic patients who are at risk of having an aneurysm because of a strong family history of aneurysmal subarachnoid hemorrhage or because of autosomal dominant polycystic kidney disease (7–9). Although screening of asymptomatic individuals without such risk factors is still controversial, MR angiography is used for screening of unruptured aneurysms in the general population in Japan (10).

To date, MR angiography is widely accepted in screening for intracranial aneurysms, and the demand is increasing. In screening for unruptured intracranial aneurysms with MR angiography, however, radiologists need to analyze large amounts of data that include multiple image projections per examination and source images obtained with MR angiography. It is time consuming and sometimes difficult for radiologists to find small aneurysms, or it may not be easy to detect medium aneurysms on maximum intensity projection (MIP) images, because of overlap with adjacent vessels and because of unusual locations (11,12). Thus, there is always the risk of missing an aneurysm. There are some methods that help avoid missing an intracranial aneurysm, such as the use of independent readings by two or more radiologists (11). Independent readings by two or more radiologists, however, increase the workload of radiologists in a routine clinical practice.

In regard to other organs, the concept of computer-aided detection (CAD) for screening of breast cancer with mammography and for screening of lung cancer with chest radiography and/or computed tomography (CT) has been applied, and the usefulness of CAD systems for the detection of cancers has been reported (13–17). To our knowledge, however, a CAD scheme has not been applied to the detection of intracranial aneurysms with MR angiography. We have been developing a CAD system for detection of intracranial aneurysms in screening with MR angiography (18). The purpose of our study, therefore, was to retrospectively evaluate the effect of CAD on radiologists' performance in the detection of intracranial aneurysms with MR angiography.

MATERIALS AND METHODS

Patient Selection

One neuroradiologist (T.H.) retrospectively selected 60 consecutive patients with unruptured intracranial aneurysms who underwent MR angiography at the Kumamoto University Hospital, Kumamoto, Japan, to evaluate possible intracranial vascular lesions between October 1999 and August 2003. The patients' data were derived from the MR imaging database of our institution. From the same database, 60 age-matched patients without intracranial aneurysms were also recruited by the same neuroradiologist. MR angiograms obtained in the 120 patients were reviewed in consensus by two experienced neuroradiologists (T.H. and Y.K., with 16 and 24 years of experience, respectively) who did not participate in the observer performance study. Our institutional review board approved this study and did not require patient informed consent.

MR Imaging

All MR imaging examinations were performed with a 1.5-T imager (Magnetom Vision; Siemens Medical Systems, Erlangen, Germany) by using a circular polarized head coil. Three-dimensional time-of-flight MR angiograms were obtained with the following parameters: 32/6 (repetition time msec/echo time msec), one signal acquired, 20° flip angle, 64-mm slab thickness, 64 partitions, 20-cm field of view, and 256 × 512 matrix. The acquisition data were converted into a 512 × 512 matrix, with a pixel size of 0.39 × 0.39 mm, by using an interpolation technique. Tilted optimized nonsaturating excitation and magnetization transfer pulses were applied for enhancement of the signals of blood flow. The slabs were placed to include the structures from the intracranial vertebral artery to the A2 branch of the anterior cerebral artery. Saturation pulses were applied cephalad so that venous blood signals were eliminated.

Selection for Observer Performance Study

Twenty-two of the 60 patients with unruptured intracranial aneurysms were further selected for an observer performance study by the same two neuroradiologists who performed the patient selection. The inclusion criteria for the patient selection were as follows: *(a)* patients with only one aneurysm were chosen, *(b)* location and size of the aneurysm were similar to the distributions in a clinical environment, and *(c)* high-quality MR angiograms were available for interpretation. There were six men and 16 women, with an age range of 43–86 years (mean age, 60.2 years). The locations and sizes of the aneurysms are listed in Table 1. The sizes of the aneurysm ranged from 3 to 26 mm in maximum diameter (mean, 7.1 mm). According to the maximum diameter, the aneurysms were classified into three groups: eight small (<5 mm), 11 medium (5–12 mm), and three large (>12 mm). The aneurysms were located at the internal carotid artery (n = 10), middle cerebral artery (n = 4), anterior cerebral artery (n = 3), basilar artery (n = 3), posterior cerebral artery (n = 1), and vertebral artery (n = 1). The 22 lesions included 20 saccular aneurysms and two fusiform aneurysms. The diagnosis was proved at CT angiography (n = 12) and conventional digital subtraction angiography (n = 3); the remaining seven aneurysms were confirmed with consensus reading of MR angiograms by the same two experienced neuroradiologists mentioned before. Source images obtained with MR angiography were also used for the confirmation. Eight of the 22 patients had old brain infarctions; intracranial steno-occlusive disease was present in two patients. An azygous anterior cerebral artery was seen in one patient with a distal anterior cerebral artery aneurysm. Meningioma and pituitary microadenoma were seen on conventional MR images in one case each. These additional lesions did not affect the interpretation of MR angiograms.

Twenty-eight of the 60 patients without intracranial aneurysms were further selected by the same two neuroradiologists as a control group for the observer study, and the age information was similar to that of the group with aneurysms. The diagnosis of no intracranial aneurysms was proved with consensus reading of MR angiograms by the two experienced neuroradiologists; source images obtained with MR angiography were also used for the diagnosis. There were 10 men and 18 women, with an age range of 32–80 years (mean age, 58.8 years). Four of the 28 patients had old brain infarctions that did not affect the image interpretation. There were no other apparent brain lesions on MR images in this control group.

TABLE 1
Location and Size of Aneurysms

Location	Size			Total No. of Patients
	Small	Medium	Large	
Internal carotid artery, top portion	0	1	0	1
Internal carotid and anterior choroidal arteries	1	0	0	1
Internal carotid and posterior communicating arteries	1	0	0	1
Internal carotid artery, first part of cisternal segment and carotid knee segment	1	1	0	2
Internal carotid and ophthalmic arteries	1	0	0	1
Internal carotid artery, carotid knee segment	1	0	0	1
Internal carotid artery, cavernous segment	0	1*	2	3
Middle cerebral artery, sphenoidal and insular segments	2	1	1	4
Anterior communicating artery	0	2	0	2
Anterior cerebral artery, distal portion	0	1	0	1
Posterior cerebral artery, distal portion	0	1	0	1
Basilar artery, top portion	0	1	0	1
Basilar and anterior inferior cerebellar arteries	0	1	0	1
Basilar artery	1	0	0	1
Vertebral artery	0	1*	0	1
Total	8	11	3	22

* Fusiform aneurysm.

TABLE 2
A_z Values for Radiologists in Detection of Intracranial Aneurysms

Observers	Without CAD	With CAD
Neuroradiologists		
1	0.939	0.964
2	0.986	0.994
3	0.989	0.998
4	0.969	0.970
5	0.969	0.984
6	0.952	0.993
7	0.942	1.000
8	0.958	0.967
Mean	0.963	0.984
General radiologists		
9	0.916	0.961
10	0.909	0.984
11	0.871	0.978
12	0.909	0.989
13	0.871	0.989
14	0.872	0.984
15	0.910	0.993
Mean	0.894	0.983
Overall	0.931	0.983

Computerized Scheme for Automated Detection of Intracranial Aneurysms

Details of the CAD scheme used in this study are shown elsewhere (18). First, the isotropic images from three-dimensional MR angiography were processed by using three selective filters for enhancement of aneurysms, vessels, and vessel walls. The initial candidates were identified by using a multiple gray-level threshold technique on the three-dimensional dot-enhanced images within the search area, which was determined with dilatation of major vessels, because most aneurysms appear in specific vessels. Candidate regions were segmented by using a region-growing technique with monitoring of some image features. In the next step, all candidates were classified into four types according to the size of the aneurysms and the local structures involved. In each group, a number of nonaneurysms were removed by using rules that were based on localized image features related to gray levels and morphologic characteristics. Finally, linear discriminant analysis was employed for further removal of some false-positive findings. Our scheme achieved a sensitivity of 100% (36 of 36), with 0.55 false-positive finding per patient in a consistency test (18).

Observer Performance Study

A total of 15 observers, including eight board-certified radiologists who specialized in neuroradiology (neuroradiologists) (M.K., M.Y.) and seven board-certified radiologists who did not specialize in neuroradiology (general radiologists), took part in the observer performance study. All observers were blinded to the results of the diagnosis obtained from the consensus of the two experienced neuroradiologists (T.H., Y.K.). The neuroradiologists had 8–17 years of experience (mean, 13.0 years), and the general radiologists had 7–20 years of experience (mean, 13.3 years). The sequential test method (19) was used in the observer performance study. Each observer read the MR angiograms displayed on a monitor first without the computer output and rated his or her confidence level in determining the presence or absence of an aneurysm. Next, the computer output, marked by circles that indicated potential aneurysms, was superimposed on the MR angiograms. The observer then viewed the image with the computer output and rated it again. An interface program was created for an image display without and with the computer output for the observer performance test. The 15 observers viewed the MIP MR angiograms displayed on a gray-scale monitor (Precision 650; Dell, Round Rock, Tex) with a spatial resolution of 1600 × 1200. The monitor screen was divided into two areas: one area in which MR angiograms were displayed in z-axis, x-axis, and y-axis rotations and another area in which observers indicated their confidence levels in the observer performance study. On the monitor, observers could see 19 MIP MR angiograms ranging from −90° to +90° (10° intervals) in the z-axis rotation and five MIP MR angiograms ranging from −20° to +20° (10° intervals) in the x-axis and y-axis rotations. The observers were allowed to select the direction of the MR angiograms and the magnification of the images on the monitor. They were also permitted to use the cine mode for displaying the images.

Images in all of the 50 patients (22 with aneurysms and 28 without aneurysms) selected for the observer performance study were presented in the same randomized order to the observers. The observers were provided with the following information before the observer performance test: *(a)* the sequential test method that was used, *(b)* there was only one aneurysm in each patient, and *(c)* the type of aneurysm was either saccular or fusiform. The observers were blinded to the number of patients with aneurysms and the performance level of the CAD scheme. There was no limit on the reading time.

Before the observer performance test, each observer underwent a training session with four training cases to become familiar with the computer output and the test procedure. The four training cases were not included with the images from the 50 selected patients used in the

observer performance study. Each observer used a continuous rating scale of a line-marking method to rate his or her confidence level on the monitor. At the left end of the line, a confidence level that an aneurysm was definitely absent was indicated, whereas at the right end, a confidence level that an aneurysm was definitely present was indicated. Intermediate levels of confidence were indicated by the different positions on the line between the two ends, and positions close to the right and left ends indicated, respectively, greater and lesser degrees of confidence in regard to the presence of an aneurysm. The distance between the left end and the marked point was automatically determined in the computer and was converted to a confidence level that could range from 0 to 100.

To investigate the effect of CAD further, we also determined the difference between the confidence levels without and with the computer output. We assumed that a clinically relevant change in confidence levels occurred only when the difference was greater than 20 units on a 0–100 confidence rating scale. A shift of more than 20 units in the direction toward a correct diagnosis implied that the use of the CAD was beneficial. Similarly, a shift of more than 20 units in the direction toward an incorrect diagnosis implied that the use of CAD was detrimental. The number of cases with beneficial effects and the number of those with detrimental effects, according to each observer, were assessed.

Statistical Analysis

Observer performance was evaluated by using receiver operating characteristic analysis with the LABROC program, according to Metz et al (20). The receiver operating characteristic curves for each observer without and with the computer output indicated the true-positive fraction to the false-positive fraction at each confidence level. The area under the receiver operating characteristic curve (A_z) was used for comparing the observers' performance in the detection of intracranial aneurysms.

To investigate the effect of CAD for all observers, the significance of the difference between the A_z values obtained without and with CAD was evaluated by using the Wilcoxon matched-pairs signed rank test. To investigate the effect of CAD for each radiologist group, the significance of the difference in A_z values between neuroradiologists and general radiologists was evaluated with a Mann-Whitney U test. In addition, the difference between the average numbers of cases affected beneficially and detrimentally because of CAD was analyzed by using the Wilcoxon matched-pairs signed rank test. In all the analyses, a P value of less than .05 was considered to indicate a significant difference.

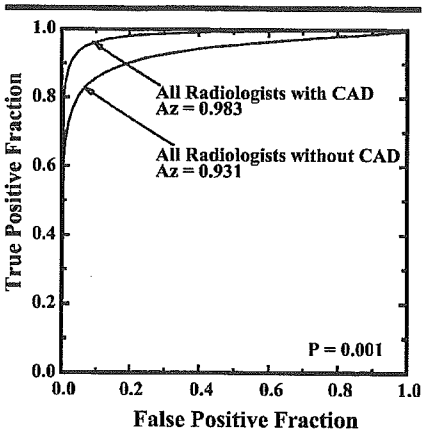

Figure 1. Graph shows average receiver operating characteristic curves for all observers in the detection of intracranial aneurysms without and with CAD output. The average A_z value in the detection of aneurysms was significantly improved from 0.931 to 0.983 when observers used the computer output (P = .001).

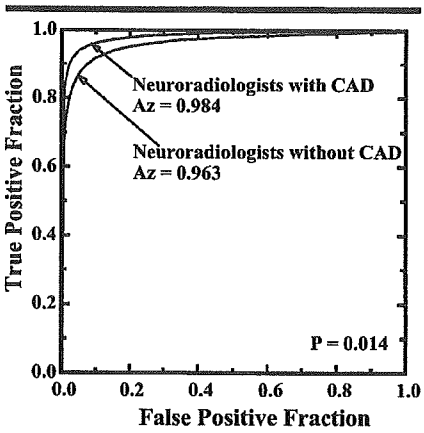

Figure 2. Graph shows average receiver operating characteristic curves for eight neuroradiologists in the detection of intracranial aneurysms. The average A_z value in detection of aneurysms was improved significantly from 0.963 to 0.984 when they used the computer output (P = .014).

RESULTS

Observer Performance

For all observers, the mean A_z values (Fig 1, Table 2) obtained without and with CAD were 0.931 ± 0.04 (standard deviation) and 0.983 ± 0.01, respectively, which indicated a significant difference (P = .001). In the neuroradiologist group (Fig 2), the mean A_z values obtained without and with CAD were 0.963 ± 0.02 and 0.984 ± 0.01, respectively, which indicated a significant difference (P = .014). In the general radiologist group (Fig 3), the mean A_z values obtained without and with CAD were 0.894 ± 0.02 and 0.983 ± 0.01, respectively, which indicated a significant difference (P = .022). There was a significant difference in the mean A_z values obtained without CAD between the two groups of radiologists (P = .001). There was no significant difference, however, in the mean A_z values obtained with CAD between the two groups of radiologists (P = .522). The performance of general radiologists (A_z = 0.983) with CAD slightly exceeded that of neuroradiologists (A_z = 0.963) without CAD. There was a significant difference in the mean A_z values between the general radiologist group with CAD and the neuroradiologist group without CAD (P = .048).

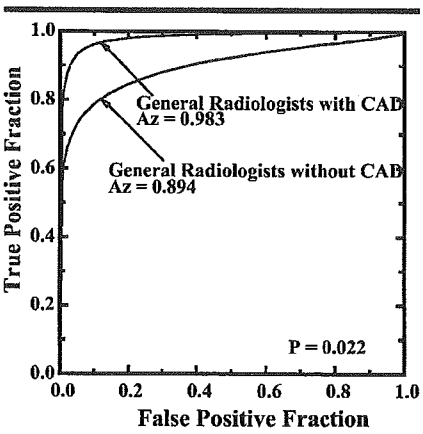

Figure 3. Graph shows average receiver operating characteristic curves for seven general radiologists in the detection of intracranial aneurysms. The average A_z value in detection of aneurysms was improved significantly from 0.894 to 0.983 when they used the computer output (P = .022).

Confidence Ratings

The results of a clinically relevant change in confidence ratings for each observer (Figs 4, 5) showed that among the 22 patients with aneurysms, the average number of cases affected beneficially was 2.3 (10%). There were no cases of patients with an aneurysm that were affected detrimentally. Among the 28 patients with-

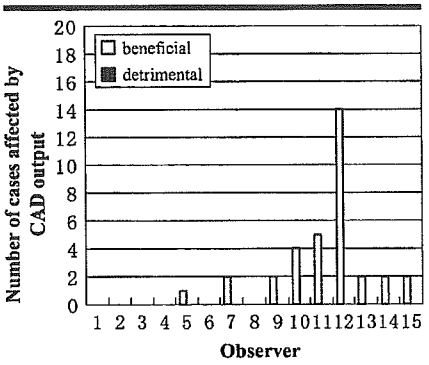

Figure 4. Graph shows number of cases (>20%) affected by the CAD output in confidence level with regard to patients with aneurysms. There were no cases affected detrimentally. The numbers *1–8* on x-axis represent the eight neuroradiologists and *9–15* represent the seven general radiologists.

TABLE 3
Summary of Aneurysms Affected Beneficially by CAD

Observers and Location	Size (mm)	No. of Cases
Neuroradiologists		
Internal carotid and anterior choroidal arteries	3	2
Internal carotid and posterior communicating arteries	4	1
General radiologists		
Internal carotid and anterior choroidal arteries	3	5
Internal carotid artery, carotid knee segment	3	1
Middle cerebral artery, sphenoidal and insular segments	4	9
Internal carotid and ophthalmic arteries	4	2
Internal carotid and posterior communicating arteries	4	1
Basilar artery	4	1
Internal carotid artery, top portion	5	2
Internal carotid artery, first part of cisternal segment and carotid knee segment	5	1
Anterior communicating artery	5	1
Posterior cerebral artery, distal portion	5	1
Anterior cerebral artery, distal portion	6	1
Vertebral artery*	6	3
Internal carotid artery, cavernous segment	16	3

* Fusiform aneurysms.

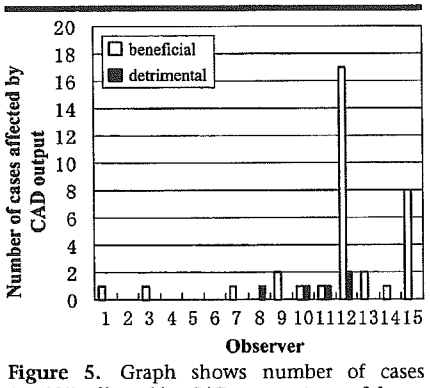

Figure 5. Graph shows number of cases (>20%) affected by CAD output in confidence level with regard to patients without aneurysms. The numbers *1–8* on x-axis represent the eight neuroradiologists, and *9–15* represent the seven general radiologists.

out aneurysms, the average number of cases that were affected beneficially was significantly larger than that of cases that were affected detrimentally (mean number of cases, 2.3 [8%] vs 0.3 [1%]; P = .02).

In beneficially affected cases in patients with aneurysms, small aneurysms at the internal carotid artery were frequently affected in both the neuroradiologist and general radiologist groups (Table 3). The general radiologists were more likely to be affected with small aneurysms at the middle cerebral artery, medium aneurysms at an unusual location such as the distal anterior and posterior cerebral arteries, medium fusiform aneurysms at the vertebral artery, and large aneurysms at the internal carotid artery. Large aneurysms at the internal carotid artery were missed in the first rating by three general radiologists because the signal intensity of the large aneurysm was relatively low as a result of turbulent flow within the aneurysm. In the five detrimentally affected cases in patients without aneurysms, the detrimental effects in both groups were caused by an increase in the confidence level in favor of the presence of an aneurysm.

DISCUSSION

We analyzed A_z values separately for neuroradiologists and general radiologists to determine whether the effect of CAD on observer performance was dependent on clinical experience. The results indicated that the use of computer output was more beneficial to general radiologists than it was to neuroradiologists; the A_z values for general radiologists with CAD were almost equal to those for neuroradiologists. In addition, it is important to note that the effect of using the computer output was also beneficial for neuroradiologists.

The knowledge required for detection of intracranial aneurysms with MR angiography includes the anatomy of the intracranial vessels, common locations of intracranial aneurysms, etiology and classification of the aneurysms, diagnostic accuracy of MR angiography for intracranial aneurysms, and artifacts and pitfalls for MR angiography. All of the general radiologists who took part in the observer study had limited experience, of 1 year or less, in neuroradiology, and were considered to be unfamiliar with findings of intracranial aneurysms. This factor presumably accounts for the finding that general radiologists benefited much more from the use of CAD. In other words, the radiologist's performance in detection of intracranial aneurysms probably depends on his or her experience and knowledge as a neuroradiologist. The fact that the effect of using CAD for neuroradiologists was also beneficial, however, may indicate that the use of CAD can improve radiologists' detection performance irrespective of their knowledge and experience.

In our study, 10% of cases in patients with aneurysms were affected beneficially by the computer output. This result was caused by an increase in the observer's confidence in diagnosing the presence of aneurysms in cases in patients with aneurysms that were detected with the use of CAD. It is sometimes difficult for radiologists to find small aneurysms, or it may not be easy to detect medium aneurysms on MIP images because of overlap with adjacent vessels and because of unusual locations (11,12). Our results without use of CAD showed a similar tendency for the false-negative findings with MIP MR angiograms. We also found that large aneurysms might be missed by general radiologists. Because general radiologists are not familiar with the unusual signal intensity of large aneurysms on MR angiograms, they might have missed these aneurysms.

Our observer performance test results indicated that the use of CAD was clearly beneficial, even in cases in patients without aneurysms. About 8% of cases in pa-

tients without aneurysms were affected beneficially because of the increase in the observer's confidence in diagnosing the absence of aneurysms in cases in patients without aneurysms. On the other hand, only 1% of cases in patients without aneurysms were affected detrimentally because of an increase in the confidence level in favor of the presence of an aneurysm. The detrimental effects were significantly smaller than were the beneficial effects. Unruptured intracranial aneurysms are being diagnosed with greater frequency as imaging technologies improve. Since the workload of radiologists will increase in the near future, the use of CAD may be necessary to increase true-positive findings and decrease false-positive findings as interpreted by radiologists.

Our study had limitations. First, source images obtained with MR angiography were not included in this observer performance study. It is likely that source images obtained with MR angiography would have been helpful in the detection of aneurysms. Reading source images obtained with MR angiography, however, may be time consuming for radiologists, especially for general radiologists. Because the fatigue in reading many images for observer performance testing may affect the results, we used only MIP images obtained with MR angiography in this study. We provided multiple views of MIP images to observers. Therefore, we believe that this observer performance test was adequate for assessment of observer performance in the detection of aneurysms. Second, this study might have had a bias in patient selection. We selected 22 patients with aneurysms and 28 control patients. The aneurysms were of various sizes, but most were small or medium, and nearly half were small. In addition, some aneurysms were located at unusual sites. Patients with steno-occlusive disease were also included to simulate patients in our routine practice. Thus, we believe that the patients we selected reflected patients seen in routine clinical practice. Third, there was a difference between the observer performance study and a clinical environment. We provided observers with the information in regard to the number of aneurysms in patients with aneurysms. Provision of such information may have affected observer performance. Although readers considered that multiple aneurysms may have existed on a given image, they indicated one aneurysm with confidence, because they knew that only one aneurysm was present in a patient with an aneurysm in the observer performance study. Thus, potential false-positive reports might have been artificially excluded.

In conclusion, the use of our CAD system helped to improve both neuroradiologists' and general radiologists' performance in the detection of intracranial aneurysms with MR angiography, and this improvement was more marked for general radiologists than it was for neuroradiologists. Further investigations about the usefulness of the CAD scheme, as applied to various MR angiograms with various MR imaging units, are needed for application in routine clinical practice.

Acknowledgments: We are grateful to the following personnel for their help: Shoji Morishita, MD, Yoshiko Hayashida, MD, Ryuji Murakami, MD, Ichiro Ikushima, MD, Yoshinori Shigematsu, MD, Takeshi Sugahara, MD, Tomoko Okuda, MD, Shingo Kakeda, MD, Takatoshi Aoki, MD, Koichi Kawanaka, MD, Yoshiharu Nakayama, MD, Masanori Imuta, MD, and Ichiro Ogata, MD, for their participation in this observer study; Junji Shiraishi, PhD, for receiver operating characteristic analysis; Roger Engelmann, MS, for development of the software used in this observer study; Ryuji Ikeda for data management; and Elisabeth Lanzl for English wording.

References

1. Wardlaw JM, White PM. The detection and management of unruptured intracranial aneurysms. Brain 2000;123:205–221.
2. International Study of Unruptured Intracranial Aneurysms Investigators. Unruptured intracranial aneurysms: risk of rupture and risks of surgical intervention. N Engl J Med 1998; 339:1725–1733.
3. Chang HS, Kirino T. Quantification of operative benefit for unruptured cerebral aneurysms: a theoretical approach. J Neurosurg 1995;83:413–420.
4. Leblanc R, Worsley KJ. Surgery of unruptured, asymptomatic aneurysms: a decision analysis. Can J Neurol Sci 1995;22: 30–35.
5. International Study of Unruptured Intracranial Aneurysms Investigators. Unruptured intracranial aneurysms: natural history, clinical outcome, and risks of surgical and endovascular treatment. Lancet 2003; 362:103–110.
6. White PM, Wardlaw JM, Easton V. Can noninvasive imaging accurately depict intracranial aneurysms? a systematic review. Radiology 2000;217:361–370.
7. Ruggieri PM, Poulos N, Masaryk TJ, et al. Occult intracranial aneurysms in polycystic kidney disease: screening with MR angiography. Radiology 1994;191:33–39.
8. Ronkainen A, Puranen MI, Hernesniemi JA, et al. Intracranial aneurysms: MR angiographic screening in 400 asymptomatic individuals with increased familial risk. Radiology 1995;195:35–40.
9. Raaymakers TW, Buys PC, Verbeeten B Jr, et al. MR angiography as a screening tool for intracranial aneurysms: feasibility, test characteristics, and interobserver agreement. AJR Am J Roentgenol 1999;173:1469–1475.
10. Baba Y, Takahashi M, Korogi Y. Cost-effectiveness of screening unruptured cerebral aneurysms in Japan. Eur Radiol 2000; 10: S362–S365.
11. Korogi Y, Takahashi M, Mabuchi N, et al. Intracranial aneurysms: diagnostic accuracy of three-dimensional, Fourier transform, time-of-flight MR angiography. Radiology 1994;193:181–186.
12. Korogi Y, Takahashi M, Mabuchi N, et al. Intracranial aneurysms: diagnostic accuracy of MR angiography with evaluation of maximum intensity projection and source images. Radiology 1996;199:199–207.
13. Freer TW, Ulissey MJ. Screening mammography with computer-aided detection: prospective study of 12,860 patients in a community breast center. Radiology 2001;220: 781–786.
14. Destounis SV, DiNitto P, Logan-Young W, Bonaccio E, Zuley ML, Willison KM. Can computer-aided detection with double reading of screening mammograms help decrease the false-negative rate? initial experience. Radiology 2004;232:578–584.
15. MacMahon H, Engelmann R, Behlen FM, et al. Computer-aided diagnosis of pulmonary nodules: results of a large-scale observer test. Radiology 1999;213:723–726.
16. Shiraishi J, Abe H, Engelmann R, Aoyama M, MacMahon H, Doi K. Computer-aided diagnosis to distinguish benign from malignant solitary pulmonary nodules on radiographs: ROC analysis of radiologists' performance—initial experience. Radiology 2003;227:469–474.
17. Awai K, Murao K, Ozawa A, et al. Pulmonary nodules at chest CT: effect of computer-aided diagnosis on radiologists' detection performance. Radiology 2004;230: 347–352.
18. Arimura H, Li Q, Korogi Y, et al. Automated computerized scheme for detection of unruptured intracranial aneurysms in three-dimensional MRA. Acad Radiol 2004;11:1093–1104.
19. Kobayashi T, Xu XW, MacMahon H, Metz CE, Doi K. Effect of a computer-aided diagnosis scheme on radiologists' performance in detection of lung nodules on radiographs. Radiology 1996;199:843–848.
20. Metz CE, Herman BA, Shen JH. Maximum-likelihood estimation of receiver operating (ROC) characteristic curves from continuously-distributed data. Stat Med 1998;17: 1033–1053.

AJNR Am J Neuroradiol 26:2243–2247, October 2005

Postoperative Assessment of Extracranial–Intracranial Bypass by Time-Resolved 3D Contrast-Enhanced MR Angiography Using Parallel Imaging

Kazuhiro Tsuchiya, Keita Honya, Akira Fujikawa, Hidekatsu Tateishi, and Yoshiaki Shiokawa

PURPOSE: **Our goals were to assess image quality of time-resolved contrast-enhanced MR angiography (CE MRA), by using 3D data acquisition along with a parallel imaging technique that can improve temporal resolution and to compare this technique with 3D-time-of-flight (TOF) MRA in the postoperative assessment of extracranial (EC)–intracranial (IC) bypass surgery.**

METHODS: **On a 1.5T imaging system, we performed CE MRA by using a 3D fast field-echo sequence in combination with a parallel imaging technique, to obtain images in the coronal plane centered at the postoperative site. Our patient group comprised 17 patients, including 13 after superficial temporal artery–middle cerebral artery (MCA) anastomosis, 3 after external carotid artery-MCA anastomosis, and one after extracranial vertebral artery–posterior cerebral artery anastomosis. Visualization of the anastomosis and the distal flow on the CE-MRA images was assessed comparatively with that on 3D-TOF MR angiograms obtained at the same time. In 6 patients, we also compared the efficiency of visualization on CE-MRA images with that on conventional angiograms.**

RESULTS: **A temporal resolution of 0.8 s/frame could be achieved with the technique employed. The bypass was better demonstrated postoperatively on CE-MRA images than on 3D-TOF MR angiograms in 13 patients (76%), whereas the 2 methods were equivalent in 4 patients (24%). Good correspondence of results was observed in the 6 patients for whom CE MRA and conventional digital subtraction angiography (DSA) images were compared.**

CONCLUSION: **CE MRA by using the parallel imaging technique can increase image acquisition speed with sufficient image quality. This technique is at least equivalent to 3D-TOF MRA to evaluate the postoperative status of EC-IC bypass.**

Extracranial–intracranial (EC-IC) bypass surgery has been used to increase the cerebral blood flow and halt extension of the affected area or reduce the risk of future strokes in patients with ischemic cerebrovascular disease (1–3). Furthermore, several kinds of bypass surgery are performed in patients with cerebral aneurysm, in which the parent artery often has to be sacrificed. In these cases, conventional angiography has been used as the most reliable method to assess the patency of the EC-IC anastomosis postoperatively. Recently, however, several other modalities—including MR angiography (MRA), sonography, and CT angiography—have also been reported to be useful for such assessment (4–7).

Time-resolved contrast-enhanced (CE) MRA, in which a rapid T1-weighted sequence is performed in combination with bolus intravenous injection of a gadolinium-based contrast agent, provides useful anatomic and hemodynamic information concerning intracranial vascular lesions. To generate "time-resolved" images, 2D sequences were previously used (8–14). More recently, however, a technique using an effective k-space sampling technique that provides good temporal resolution even with 3D data acquisition has been reported (15). Multiple arrays of receiver coils are used in the parallel imaging tech-

Received January 13, 2005; accepted after revision March 22.

From the Departments of Radiology (K.T., K.H., A.F.) and Neurosurgery (H.T., Y.S.), Kyorin University School of Medicine, Tokyo, Japan.

Presented as "Postoperative Assessment of External Carotid-Internal Carotid Bypass by MR Digital Subtraction Angiography Using Parallel Imaging"at the 42nd annual meeting of the American Society of Neuroradiology, June 7–11, 2004, Seattle, WA.

Address correspondence to Kazuhiro Tsuchiya, MD, Department of Radiology, Kyorin University School of Medicine, 6-20-2, Shinkawa, Mitaka, Tokyo 181-8611, Japan.